Smoothed particle simulation of gravity waves in a multi-fluid system

Songdong Shao MSc, PhD, FHEA
Senior Lecturer in Environmental Fluid Mechanics, School of Engineering, Design and Technology,
University of Bradford, UK

The generation and propagation of gravity waves in a multi-fluid system have significant environmental impacts. This paper presents an incompressible smoothed particle hydrodynamics model to simulate this process. The method is a mesh-free particle modelling approach that can treat the free surfaces and multi-interfaces in a straightforward manner. The proposed model is based on the general multi-fluid flow equations and uses a unified pressure formulation to address the interactions among the different components of the fluids. The model will be used to investigate the gravity currents generated from one fluid intruding into other fluids with different densities. The general features of the gravity current have been disclosed and the computed gravity wave height and wave propagation speed agree well with the theoretical analysis. The error analysis proved the convergence of the numerical scheme and it was found that the multi-fluid model is close to first-order accurate.

Notation

a^*	wave amplitude generated by gravity current
c	solitary wave celerity
D	depth of lock fluids
d	water depth
$\boldsymbol{f}_{ls}$	interaction force vector among different fluids
$\boldsymbol{g}$	gravitational acceleration vector
g'	effective gravity
h	smoothing distance
k	empirical coefficient for current head velocity
m	particle mass
P	pressure
$\boldsymbol{r}$	position vector
$\boldsymbol{r}^*$	intermediate position vector
Δt	time increment
$\boldsymbol{u}$	velocity vector
$\Delta\boldsymbol{u}^*$	velocity increment in prediction step
$\Delta\boldsymbol{u}^{**}$	velocity increment in correction step
v_h	current head velocity
W	interpolation kernel
ΔX	particle spacing
ε	relative error in wave amplitude
η	solitary wave surface elevation
μ	dynamic viscosity of laminar flow
ρ	fluid density
ρ_0	averaged density of current head
ρ^0	initial constant density
ρ^*	intermediate density
$\Delta\rho_B$	density difference between bottom and upper fluids

Subscripts

a	reference particle
b	neighbouring particle
l	liquid component
m	different fluids component
s	solid component
t	time
x	horizontal coordinate
y	vertical coordinate

1. Introduction

The gravity current is the flow of a fluid of one density intruding into another fluid with a different density under the influence of gravity. During this process, the gravity waves can be generated and propagate a long distance downstream, which could have a significant impact on the environmental flow system. In early studies, most researchers had to rely on analytical and experimental approaches to gain the basic physical mechanisms of the gravity flows owing to the complexity of the problem, such as Britter and Linden (1980) and Rottman and Simpson (1983). Nowadays, computer simulation techniques have provided a robust tool to study such a complicated process and they can disclose detailed flow information about the interface deformation, velocity structure, extensive mixing and entrainment and so on. For example, some established numerical models based on the Navier–Stokes equations have been used by Firoozabadi *et al.* (2003), Imran *et al.* (2004) and Patterson *et al.* (2005). Besides, Monaghan *et al.* (1999) and Monaghan (2007) have

Engineering and Computational Mechanics
Volume 166 Issue EM1

Smoothed particle simulation of gravity
waves in a multi-fluid system
Shao

given a full summary on the experimental and numerical approaches in this area.

The smoothed particle hydrodynamics (SPH) method is one highly robust particle modelling technique that was originally developed for astrophysical flows (Monaghan, 1992) and has since been modified for many kinds of incompressible free surface flows. Based on the weakly compressible SPH (WCSPH) algorithm, in which the fluid was treated as being slightly compressible, a variety of multi-fluid SPH models have been developed, such as for the dust gas flows (Monaghan and Kocharyan, 1995), gravity currents (Monaghan et al., 1999) and interfacial flows (Colagrossi and Landrini, 2003). The incompressible SPH (ISPH) modelling approach was developed based on the classic WCSPH but uses a strict hydrodynamic formulation to compute the fluid pressures (Shao and Lo, 2003). The subsequent research into ISPH models found that the computational efficiency and the pressure stability have improved in the ISPH algorithm (Ataie-Ashtiani and Shobeyri, 2008; Lee et al., 2008). Thus the ISPH model is selected as a promising tool to study the gravity current waves in this paper. The original single-fluid ISPH algorithm will be further developed based on the universal multi-fluid flow equations and the complicated interactions among the different fluid components will be simply treated by a unified pressure equation. The proposed model will be applied to a lock fluid flowing down a ramp into the two different fluids based on the work of Monaghan et al. (1999).

2. Development of multi-fluid ISPH model

2.1 Governing equations

The multi-fluid ISPH model is established on the general multi-phase flow equations in the Lagrangian form. The continuity and momentum equations are written as below

$$1. \qquad \left. \begin{aligned} \frac{1}{\rho_1}\frac{d\rho_1}{\mathrm{d}t} + \nabla \cdot \boldsymbol{u}_1 = 0 \\ \frac{1}{\rho_\mathrm{s}}\frac{d\rho_\mathrm{s}}{\mathrm{d}t} + \nabla \cdot \boldsymbol{u}_\mathrm{s} = 0 \end{aligned} \right\}$$

$$2. \qquad \left. \begin{aligned} \rho_1\frac{d\boldsymbol{u}_1}{\mathrm{d}t} = -\nabla P_1 + \rho_1\boldsymbol{g} + \mu_1\nabla^2\boldsymbol{u}_1 + \boldsymbol{f}_\mathrm{ls} \\ \rho_\mathrm{s}\frac{d\boldsymbol{u}_\mathrm{s}}{\mathrm{d}t} = -\nabla P_\mathrm{s} + \rho_\mathrm{s}\boldsymbol{g} + \mu_\mathrm{s}\nabla^2\boldsymbol{u}_\mathrm{s} - \boldsymbol{f}_\mathrm{ls} \end{aligned} \right\}$$

in which ρ is density; t represents time; $\boldsymbol{u}$ is velocity; P is pressure; $\boldsymbol{g}$ denotes gravitational acceleration; μ is dynamic viscosity and $\boldsymbol{f}_\mathrm{ls}$ represents interaction forces among the different fluid components. The subscripts l and s refer to the different fluid components, or liquid and solid phases in a general term.

2.2 Solution methods

The ISPH solution methods employ a two-step prediction/correction approach to solve the governing Equations 1 and 2. The final flow velocity is calculated by using a time-marching procedure as

$$3. \qquad \boldsymbol{u}_{\mathrm{m},t+1} = \boldsymbol{u}_{\mathrm{m},t} + \Delta\boldsymbol{u}^*_{\mathrm{m},t} + \Delta\boldsymbol{u}^{**}_{\mathrm{m},t} \quad (\mathrm{m} = \mathrm{l, s})$$

in which $\Delta\boldsymbol{u}^*_{\mathrm{m},t}$ is velocity increment in the prediction step; $\Delta\boldsymbol{u}^{**}_{\mathrm{m},t}$ represents velocity increment in the correction step; $\boldsymbol{u}_{\mathrm{m},t}$ denotes velocity at time t and $\boldsymbol{u}_{\mathrm{m},t+1}$ represents velocity at time $t+1$. Here m = l, s refer to the different fluids.

The prediction step in the ISPH solutions is an explicit integration in the time without enforcing the incompressibility. In this step, only the gravitational and viscous forces in Equation 2 are used and an intermediate particle velocity and position of the multi-fluid flows are obtained

$$4. \qquad \left. \begin{aligned} \Delta\boldsymbol{u}^*_{1,t} = \left(\frac{\mu_1}{\rho_1}\nabla^2\boldsymbol{u}_1\right)_t \Delta t + \boldsymbol{g}\Delta t \\ \Delta\boldsymbol{u}^*_{\mathrm{s},t} = \left(\frac{\mu_\mathrm{s}}{\rho_\mathrm{s}}\nabla^2\boldsymbol{u}_\mathrm{s}\right)_t \Delta t + \boldsymbol{g}\Delta t \end{aligned} \right\}$$

$$5. \qquad \left. \begin{aligned} \boldsymbol{u}^*_{\mathrm{m},t} = \boldsymbol{u}_{\mathrm{m},t} + \Delta\boldsymbol{u}^*_{\mathrm{m},t} \\ \boldsymbol{r}^*_{\mathrm{m},t} = \boldsymbol{r}_{\mathrm{m},t} + \boldsymbol{u}^*_{\mathrm{m},t}\Delta t \end{aligned} \right\} \quad (\mathrm{m} = \mathrm{l, s})$$

in which Δt is time increment; $\boldsymbol{r}_{\mathrm{m}t}$ denotes particle position at time t and $\boldsymbol{r}^*_{\mathrm{m},t}$ represents intermediate particle position.

After the predictive computations, the incompressibility of the fluid system is not satisfied. This is manifested by the fact that the intermediate density of the fluid particles ρ^* deviate from the initial constant density ρ^0. Thus the densities of the particles are required to be corrected to the initial values in the correction step to satisfy the incompressibility.

The velocity increment in the correction step is calculated by

$$6. \qquad \left. \begin{aligned} \rho_1\Delta\boldsymbol{u}^{**}_{1,t} = -\nabla P_{t+1}\Delta t \\ \rho_\mathrm{s}\Delta\boldsymbol{u}^{**}_{\mathrm{s},t} = -\nabla P_{t+1}\Delta t \end{aligned} \right\}$$

Here it can be seen that the interaction terms among the different fluid components have been dropped through a unified pressure term that does not distinguish the different fluids. The detailed derivations can be found in Gotoh and Sakai (2006) in their moving particle semi-implicit (MPS) method. The unified pressure equation can be derived by combining the continuity and

Engineering and Computational Mechanics
Volume 166 Issue EM1

Smoothed particle simulation of gravity
waves in a multi-fluid system
Shao

momentum Equations 1 and 2 and represented for each of the fluid components as

$$7. \quad \nabla \cdot \left(\frac{1}{\rho_m}\nabla P_{t+1}\right) = \frac{\rho^0 - \rho^*}{\rho^0(\Delta t)^2} \quad (m = 1, s)$$

Finally, the spatial position of the fluid particles is calculated by using a central scheme in time as:

$$8. \quad r_{m,t+1} = r_{m,t} + \frac{(u_{m,t} + u_{m,t+1})}{2}\Delta t \quad (m = 1, s)$$

in which $r_{m,t+1}$ is position of the particle at time $t + 1$.

2.3 SPH theories and formulations

In an SPH framework, the modelled fluid media are discretised as an assembly of a large number of individual particles. The particle interaction zone is supposed to be around each particle. All of the terms in the governing Equations 1 and 2 are described as the interactions between the reference particle and its neighbours. Thus the computational grid is not required. Combined with the adequate initial and boundary conditions, a particular hydrodynamic problem can be solved exclusively through the particle properties. The SPH numerical scheme is free from the numerical diffusions since the advection term is calculated by the motion of the particles. Besides, the deformation of the free surfaces and multi-interfaces can easily be tracked by the particles.

In the SPH formulations, the motion of each particle is calculated through the interactions with its neighbouring particles using an analytical kernel function. The detailed reviews of the SPH principles are provided by Monaghan (1992). Among a variety of the kernels documented in the literature, the spline-based kernel normalised in two dimensions is widely used in different hydrodynamic calculations. The following standard SPH formulations are used in the proposed multi-fluid ISPH model.

The density ρ_a of a fluid particle a is calculated by

$$9. \quad \rho_a = \sum_b m_b W(|r_a - r_b|, h)$$

in which a and b are reference particle and its neighbours; m_b represents particle mass; r_a and r_b are particle positions; W is interpolation kernel and h denotes smoothing distance, which determines the range of the particle interactions.

The pressure gradient uses the following form as

$$10. \quad \left(\frac{1}{\rho}\nabla P\right)_a = \sum_b m_b \left(\frac{P_a}{\rho_a^2} + \frac{P_b}{\rho_b^2}\right)\nabla_a W_{ab}$$

in which the summation is over all the particles other than particle a and $\nabla_a W_{ab}$ represents the gradient of the kernel taken with respect to the position of particle a.

The Laplacian for the pressure term and the laminar viscosity are formulated as a hybrid of a standard SPH first derivative combined with a finite difference approximation for the first derivative. The purpose is to eliminate the numerical instability caused by the particle disorders arising from the second derivative of the SPH kernel (Shao and Lo, 2003). They are represented in the following symmetrical forms to conserve the particle properties

$$11. \quad \nabla \cdot \left(\frac{1}{\rho}\nabla P\right)_a = \sum_b m_b \frac{8}{(\rho_a + \rho_b)^2} \\ \times \frac{(P_a - P_b)(r_a - r_b)\cdot\nabla_a W_{ab}}{|r_a - r_b|^2}$$

$$12. \quad \left(\frac{\mu}{\rho}\nabla^2 u\right)_a = \sum_b m_b \frac{2[(\mu_a/\rho_a) + (\mu_b/\rho_b)]}{\rho_a + \rho_b} \\ \times \frac{(u_a - u_b)(r_a - r_b)\cdot\nabla_a W_{ab}}{|r_a - r_b|^2}$$

3. Boundary conditions, free surfaces and multi-interfaces

3.1 Impermeable solid walls

In the ISPH numerical scheme, the solid walls are modelled by the fixed wall particles that balance the pressures of the inner fluid particles and prevent them from penetrating the wall. The pressure Poisson Equation 7 is solved on these wall particles. When an inner fluid particle approaches the wall, the pressure of the wall particles increases, and vice versa. For details, see Shao and Lo (2003).

3.2 Free surfaces and multi-interfaces

The free surfaces can be easily and accurately tracked by using the fluid particles. As there is no fluid particle existing in the outer region of the free surface, the particle density on the free surface should drop significantly. This criterion is used to judge the surface particles and a zero pressure is given to each of the surface particles when solving the pressure Poisson Equation 7.

For a multi-fluid flow simulation, the interfaces between the different fluids can also be identified by using the particle densities. If the density of a particle falls between the densities of

Engineering and Computational Mechanics
Volume 166 Issue EM1

Smoothed particle simulation of gravity
waves in a multi-fluid system
Shao

a lighter fluid and a heavier fluid, this particle is then recognised as an interface particle. It is obvious that the ISPH model can also describe the multi-interfaces in a straightforward manner without involving the complicated front-tracking algorithms that are commonly used in a grid method.

4. Model validation

The proposed multi-fluid ISPH model is first validated by a discontinuous density current flowing down a sloping bed based on the experimental and numerical work of Cantero *et al.* (2003). The numerical settings of the flume geometry and two different fluids are shown in Figure 1. The salty water with a density of 1007 kg/m^3 is released to the ambient water with a density of 1000 kg/m^3 over a slope of 0·08. In the ISPH computations, a shorter computational domain of 7·0 m is used to save the central processing unit (CPU) time. The initial particle spacing is chosen as $\Delta X = 0·01$ m and thus the total computational particles include 43 050 water particles and 1336 salty water particles. In Cantero *et al.* (2003), this problem was solved by using the RANS model with a discontinuity front capturing technique based on a finite-element solver and the computations were compared with the experiment performed by Professor Marcelo H. Garcia (Cantero *et al.*, 2003).

To validate the ISPH modelling accuracy, the computed time-dependent leading edge of the density current front is compared with the experimental data and computational fluid dynamics (CFD) results of Cantero *et al.* (2003) in Figure 2. It shows that the general agreement among the three data sets is satisfactory. The CFD results overpredict the experimental leading edge before time $t = 50$ s but underpredict it after $t = 75$ s. In contrast, the ISPH computations underpredict the experiment at the beginning of the computation but are more close to the experiment at the later stage of the density current flow. The maximum error between the ISPH results and the experimental data is 6·2%, while it is 11·7% for the CFD simulations of Cantero *et al.* (2003). Here it should be mentioned that Cantero *et al.* (2003) used a mesh system with 45 676 nodes and 45 000 bilinear quadrilateral elements to reproduce the experiment that has a similar spatial accuracy as the ISPH particle resolutions.
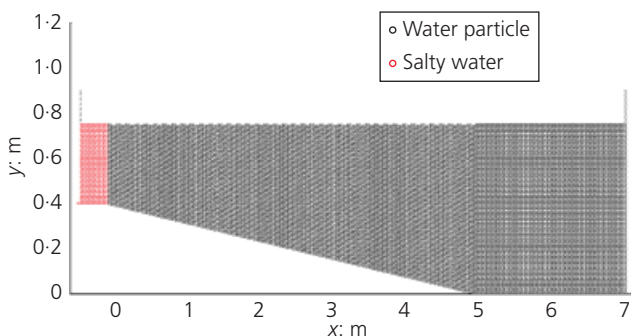
Figure 1. Numerical tank set-up with two different fluids based on Cantero *et al.* (2003)
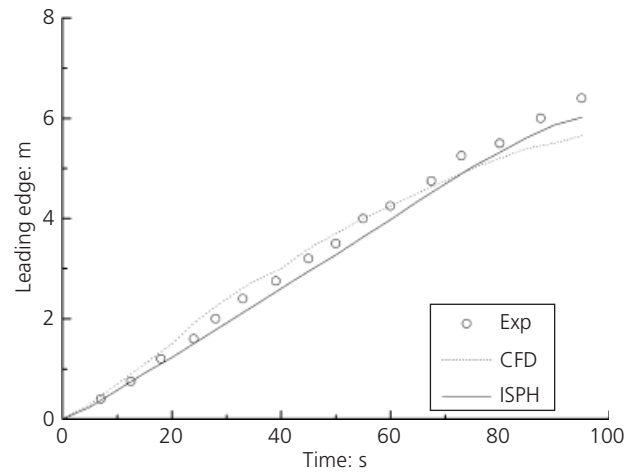
Figure 2. Experimental and numerical time-dependent leading edge of density current front computed by ISPH and CFD solver (Cantero *et al.*, 2003)

5. Model application – gravity current flowing down a ramp into stratified fluids

5.1 Numerical tank settings

Many of the gravity currents that happen in a practical field involve the flows into a density-stratified fluid field. The interface of the stratified fluids can have several effects on the gravity current, such as diverting the flow and initiating a large amplitude solitary wave that can have harmful influences over a long distance (Monaghan *et al.*, 1999).

To investigate a practical situation, we now consider a mild ramp with 20° slope, consisting of the lock region, horizontal section and ramp. The lock fluids have a density of 1210 kg/m^3 and the lower tank fluids have a density of 1070 kg/m^3 overlaid by a fresh water layer with a density of 1000 kg/m^3. According to the numerical settings of Monaghan *et al.* (1999), the lock region has a length of 0·5 m and depth of 0·25 m. To reduce the computational cost, the left end of the tank was set 0·75 m from the bottom of the ramp. The bottom fluid layer has a depth of 0·23 m. The proposed multi-fluid ISPH model aims to reproduce the numerical results from the established WCSPH approach of Monaghan *et al.* (1999) and further investigate the velocity structures near the interface during the different fluid interactions. The initial set-up of the numerical tank for the ramp flow is shown in Figure 3.

In the ISPH computations, an initial particle spacing of $\Delta X = 0·01$ m is used by balancing the computational efficiency and accuracy. There are a total of 13 000 particles involved, consisting of the lock particles, light particles and heavy particles, as shown in Figure 3. Different types of fluid particles are given different identifiers and thus the free surfaces and interfaces

Engineering and Computational Mechanics
Volume 166 Issue EM1

Smoothed particle simulation of gravity
waves in a multi-fluid system
Shao
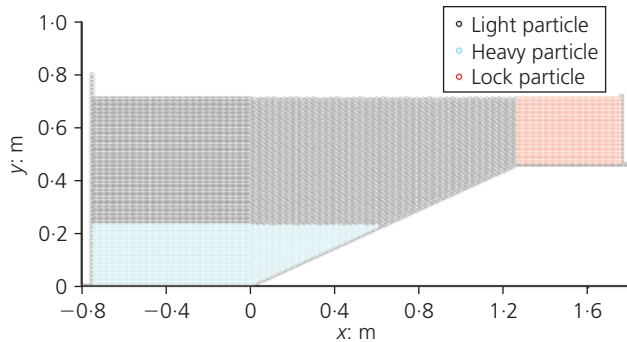
Figure 3. Initial set-up of numerical tank for gravity flow, with
three different fluids

between the different fluids can be identified throughout the
computations.

5.2   Model verifications

The computed particle snapshots during the gravity current
flowing down the ramp after the release are shown in Figures
4(a)–(c) at three different times, matching the WCSPH computa-
tions of Monaghan *et al.* (1999). The simulated flow patterns are
very similar to those shown in Figure 18 in Monaghan *et al.*
(1999). There is a qualitatively good agreement between the two
different SPH modelling approaches, and the proposed multi-fluid
ISPH model can well predict the overturning of the gravity
current head and the subsequent intruding and mixing processes.

The ISPH results predicted an averaged velocity of the gravity
current head at 0·38 m/s. An analytical value of 0·43 m/s can be
calculated by using Britter and Linden (1980)

13. $\quad v_h \sim k(g'D)^{1/2}$

in which D is the depth of the lock fluids, $g' = g\Delta\rho/\rho$ is the
effective gravity and k is an empirical coefficient in Monaghan *et
al.* (1999).

Besides, from Figure 4 the wave amplitude generated by the
descending gravity current is computed to be 0·22 m. By using
the pressure balance analysis, Monaghan *et al.* (1999) gave an
estimation of the wave amplitude at

14. $\quad a^* = \rho_0 v_h^2/\Delta\rho_B \boldsymbol{g}$

in which $\Delta\rho_B$ is the density difference between the bottom fluids
and the fresh water and ρ_0 is the averaged density of the gravity
current head. This formula gives a value of 0·23 m that is quite
close to the ISPH computations with an error of 4·3%.

To further validate the accuracy of the ISPH computations, the
analytical solitary wave profiles based on the Boussinesq equation
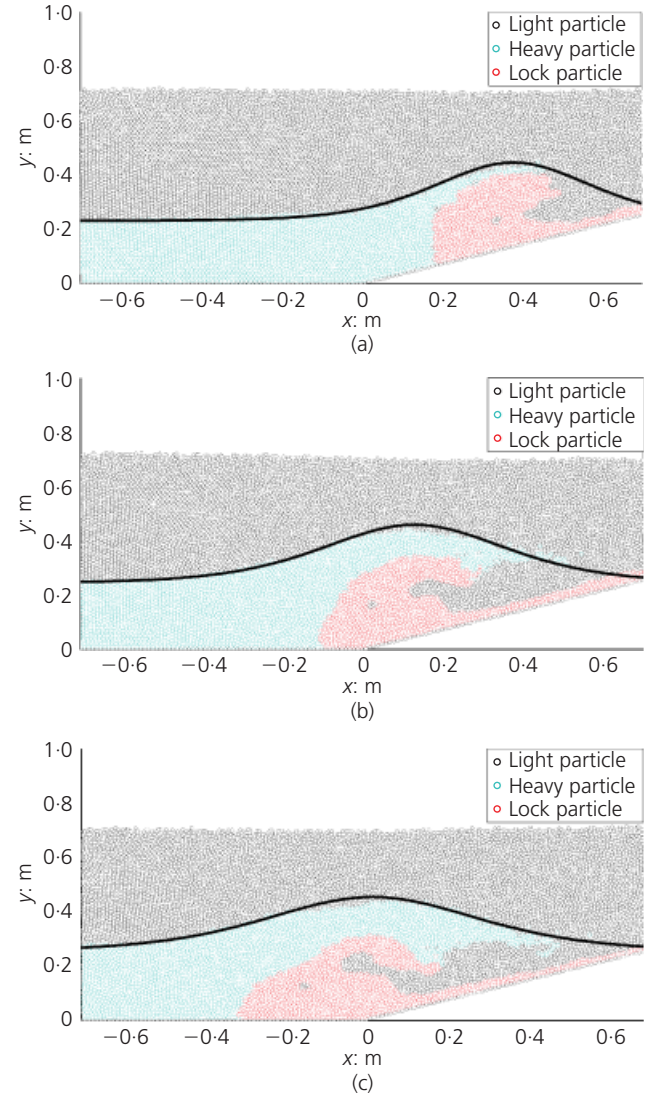
Figure 4. (a)–(c). Particle snapshots of gravity flow, with bold
lines indicating analytical solitary wave profiles: (a) $t = 3\cdot4$ s;
(b) $t = 4\cdot2$ s; (c) $t = 4\cdot7$ s

(Lee *et al.*, 1982) have also been provided in the figures for
comparison. It shows that the generated solitary waves computed
by the ISPH agree satisfactorily with the theoretical solutions,
with slight under-predictions at the wave crest. The analytical
solitary wave profile is calculated from Lee *et al.* (1982)

15. $\quad \eta(x,\ t) = a^* \sec h^2 \left[\sqrt{\dfrac{3a^*}{4d^3}}(x - ct) \right]$

in which η is wave surface elevation, d represents water depth
and $c = \sqrt{g(d + a^*)}$ is the solitary wave celerity.

Here it needs to be pointed out that the left-hand side (LHS)

Engineering and Computational Mechanics
Volume 166 Issue EM1

Smoothed particle simulation of gravity
waves in a multi-fluid system
Shao

boundary is a solid boundary that is fully reflective. The ISPH computations were stopped before the generated wave reached the LHS boundary and thus the simulated waves were not influenced by the existence of the wall.

5.3   Analysis of flow features

The computed particle snapshots in Figure 4 show that when the gravity current descends the ramp and interacts with the interface of the bottom fluids and the upper fresh water, then substantial wrapping and overturning processes occur. The current head is the main site of the intensive mixing, with the fresh water moving around and behind the head, mixing with the lock fluids. The ISPH simulations have disclosed many of the features found in the physical experiment and the numerical simulations of Monaghan *et al.* (1999). Owing to the continuous entrainment of the fresh water as the descending gravity current intrudes, the gravity current contains distinct regions mixed with the lower–higher density fluids. For example, some pockets of the fresh water are enclosed inside the lock fluid region. The gravity current has raised the interface between the bottom fluids and the fresh water by forcing the fluids in front of it to move up and around the head, generating a solitary wave. However, it should be pointed out that one difference between the ISPH and WCSPH (Monaghan *et al.*, 1999) computations is that the WCSPH predicted a plug-like gravity current head (Figure 18 in Monaghan *et al.*, 1999), while the ISPH predicted a boundary-fitted gravity current head. This is because Monaghan *et al.* (1999) used a repulsive boundary treatment while the ISPH used a hydrodynamic boundary with the Neumann conditions enforced (Shao and Lo, 2003).

Further examining the flow velocity fields in Figures 5(a)–(c), it is shown that there exists a strong flow circulation zone near the gravity current front. Owing to the sudden release of the lock fluids, the gravity current is generated and a counter-current of the fresh water flows into the lock region, producing a velocity circulation and carrying it forward as the gravity current descends the ramp. Meanwhile, the range and amplitude of the flow circulations continue to increase and the influence zones spread to the fluids further away. The ISPH simulations have disclosed a strong flow circulation over the current front and a nearly constant velocity region in the current head, which is consistent with the field and experimental observations.

The computed pressure fields of the gravity current flow at time $t = 5.7$ s are shown in Figure 6. For analysis, the interface profile of the gravity current is also shown. The figure indicates that the computed pressure fields are quite stable and there is no pressure noise near the interfaces, which is an indication that the ISPH pressure solution scheme is sound. It has also been found that the pressure contours are nearly evenly spaced within the ambient fluids and the gravity current body and the amplitude of the pressure is consistent with the current profile. That is to say, the pressure is higher inside the gravity flows that provide the momentum to move the fluid forward. This implies that the pressure distributions in a gravity current flow can be treated as a hydrostatic problem,
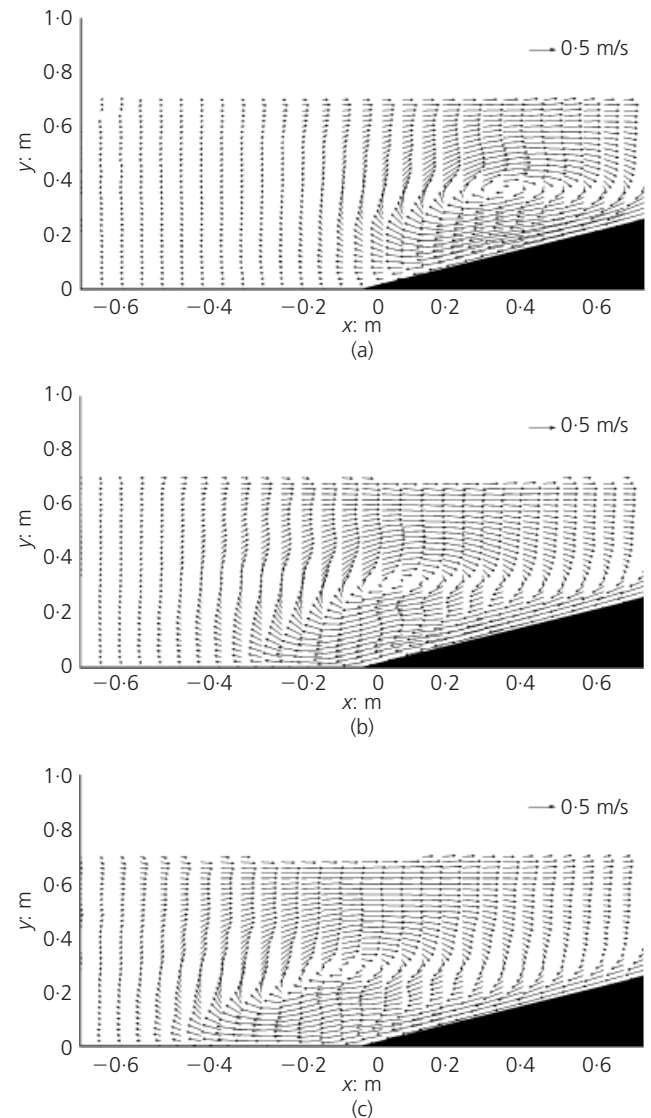
Figure 5. (a)–(c). Flow velocity fields of gravity flow, indicating flow circulations near current head: (a) $t = 3.4$ s; (b) $t = 4.2$ s; (c) $t = 4.7$ s
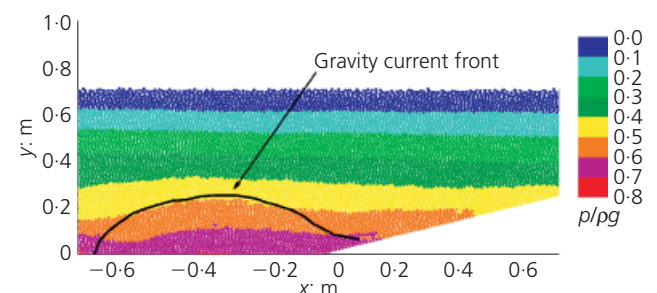
Figure 6. Computed pressure fields of gravity flow at time $t = 5.7$ s, indicating quasi-hydrostatic pressure patterns

Engineering and Computational Mechanics
Volume 166 Issue EM1

**Smoothed particle simulation of gravity
waves in a multi-fluid system**
Shao

providing a good rationale that most numerical models based on the shallow water equations (SWE) can simulate the gravity current quite well in practice (Loose *et al.*, 2005; Young *et al.*, 2005).

5.4 Numerical error analysis

To analyse the convergence behaviour of the numerical algorithm, additional computations with two different particle spacings ΔX have been made and the particle numbers used are $N = 26\,000$ and $52\,000$, respectively. The generated solitary wave is used for the analysis. The errors are calculated as the difference between the numerically generated wave amplitude and the theoretical value by using the formulation in Xu *et al.* (2009) as

16.
$$\varepsilon = \left| \frac{a^*_{num} - a^*_{analytical}}{a^*_{analytical}} \right| \times 100\%$$

The time-dependent errors in the wave amplitude computed by using the original and the additional two ISPH particle resolutions are shown in Figure 7. It clearly shows that as the particle numbers increase, that is, as the particle sizes decrease, the errors decrease rapidly indicating the convergence of the numerical scheme. The maximum errors found in the wave amplitude happen at the end of the simulations when the particle disorder is the highest. The error is 5·7% for the roughest simulation and 3·8% for the finest simulation, respectively. A simple error analysis (Shao and Lo, 2003) showed that the spatial accuracy of the multi-fluid ISPH model is close to but slightly below first-order accurate. This is less satisfactory than a single-fluid ISPH numerical scheme and more robust treatment of the interfaces would be able to further improve the spatial accuracy.

6. Conclusions

A multi-fluid ISPH model has been developed to simulate the interactions of the fluids with different densities. The model has
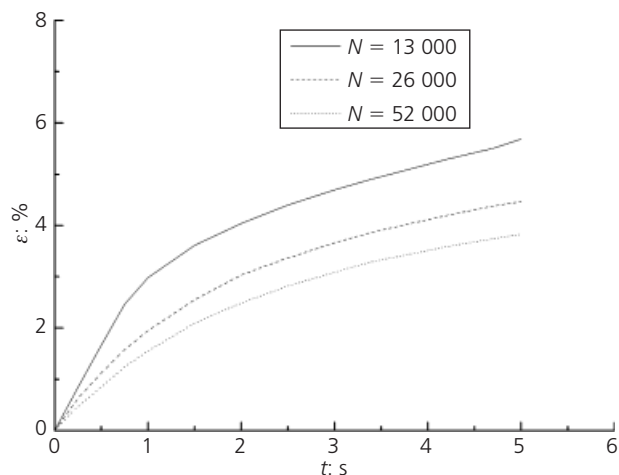
Figure 7. Time-dependent errors in wave amplitude computed by using three different particle resolutions

been validated against the case of the salty water intruding into the ambient fluids and applied to a gravity current flowing down a ramp into different fluid layers. The ISPH computations were found to be in good agreement with the documented data. The computed solitary wave celerity and wave height are consistent with the analytical results. The computed velocity fields disclose the distinct flow circulations, and the overturning and wrapping of the fluids can be naturally captured by the particle modelling approach. The computed pressure fields suggest that the pressure distributions under a gravity flow are essentially hydrostatic and thus the numerical models based on the SWE should work well for similar applications. Although further quantitative validation is required, the proposed modelling approach could provide a promising trend that is worth exploring. All of the computations were carried out on a DELL Precision T7500 with dual CPUs 3·20 GHz and RAM 48·0 G.

Also it should be noted that the latest research by Xu *et al.* (2009) indicated that by only imposing the density invariance in ISPH such as in Shao and Lo (2003) could lead to relatively large errors where the flow Reynolds number is high. This was not found in the tested cases in this paper and it could be partly attributed to the relatively smaller flow Reynolds number. More robust validations should be carried out in future to address the solver stability under a wider range of testing conditions.

REFERENCES

Ataie-Ashtiani B and Shobeyri G (2008) Numerical simulation of landslide impulsive waves by incompressible smoothed particle hydrodynamics. *International Journal for Numerical Methods in Fluids* **56(2)**: 209−232.

Britter RE and Linden PF (1980) The motion of the front of a gravity current travelling down an incline. *Journal of Fluid Mechanics* **99(3)**: 531−543.

Cantero MI, García MH, Buscaglia GC, Bombardelli FA and Dari EA (2003) Multidimensional CFD simulation of a discontinuous density current. In *Proceedings of 30th IAHR Congress, Water Engineering and Research in a Learning Society, Thessaloniki* (Ganoulis J and Prinos P (eds)). pp. 405–411.

Colagrossi A and Landrini M (2003) Numerical simulation of interfacial flows by smoothed particle hydrodynamics. *Journal of Computational Physics* **191(2)**: 448−475.

Firoozabadi B, Farhanieh B and Rad M (2003) Hydrodynamics of two-dimensional, laminar turbid density currents. *Journal of Hydraulic Research* **41(6)**: 623−630.

Gotoh H and Sakai T (2006) Key issues in the particle method for

Engineering and Computational Mechanics
Volume 166 Issue EM1

Smoothed particle simulation of gravity
waves in a multi-fluid system
Shao

computation of wave breaking. *Coastal Engineering* **53(2–3)**: 171–179.

Imran J, Kassem A and Khan SM (2004) Three-dimensional modeling of density current. Part I: flow in straight confined and unconfined channels. *Journal of Hydraulic Research* **42(6)**: 578–590.

Lee ES, Moulinec C, Xu R, *et al.* (2008) Comparisons of weakly compressible and truly incompressible algorithms for the SPH mesh free particle method. *Journal of Computational Physics* **227(18)**: 8417–8436.

Lee JJ, Skjelbreia JE and Raichlen F (1982) Measurement of velocities in solitary waves. *Journal of Waterways, Port, Coastal and Ocean Division, ASCE* **108(WW2)**: 200–218.

Loose B, Nino CY and Escauriaza MC (2005) Finite volume modeling of variable density shallow-water flow equations for a well-mixed estuary: Application to the Río Maipo estuary in central Chile. *Journal of Hydraulic Research* **43(4)**: 339–350.

Monaghan JJ (1992) Smoothed particle hydrodynamics. *Annual Review of Astronomy and Astrophysics* **30**: 543–574.

Monaghan JJ (2007) Gravity current interaction with interfaces. *Annual Review of Fluid Mechanics* **39**: 245–261.

Monaghan JJ, Cas RAF, Kos AM and Hallworth M (1999) Gravity currents descending a ramp in a stratified tank. *Journal of Fluid Mechanics* **379**: 39–69.

Monaghan JJ and Kocharyan A (1995) SPH simulation of multi-phase flow. *Computer Physics Communications* **87(1–2)**: 225–235.

Patterson MD, Simpson JE, Dalziel SB and Nikiforakis N (2005) Numerical modelling of two-dimensional and axisymmetric gravity currents. *International Journal for Numerical Methods in Fluids* **47(10–11)**: 1221–1227.

Rottman JW and Simpson JE (1983) Gravity currents produced by instantaneous releases of a heavy fluid in a rectangular channel. *Journal of Fluid Mechanics* **135**: 95–110.

Shao SD and Lo EYM (2003) Incompressible SPH method for simulating Newtonian and non-Newtonian flows with a free surface. *Advances in Water Resources* **26(7)**: 787–800.

Xu R, Stansby P and Laurence D (2009) Accuracy and stability in incompressible SPH (ISPH) based on the projection method and a new approach. *Journal of Computational Physics* **228(18)**: 6703–6725.

Young DL, Lin QH and Murugesan K (2005) Two-dimensional simulation of a thermally stratified reservoir with high sediment-laden inflow. *Journal of Hydraulic Research* **43(4)**: 351–365.